Check for updates

Flow control in a multichamber settling basin by sluice gates driven by a CFD and an ancillary analytical model

Miloš V. Nikolić and Rade M. Karamarković

ABSTRACT

Unequal flow distribution between the chambers of a three-chamber settling basin causes its malfunction and endangers the turbines of a small hydropower plant. To equalize the flows, sluice gates are used. To find their positions, the following methodologies are considered: (1) measurements combined with trial-and-error method (TAE), (2) measurements with regression analysis (RA), (3) CFD model combined with TAE, (4) CFD model with RA, (5) CFD model supported by a one-dimensional flow model, and (6) CFD model with an analytical model. The additional models and RA are intended to speed up the solution finding. From the previous list, only the sixth methodology is applicable. The first four are not because of the weir design, and the fifth because of the three-dimensional flow character. Initially, the CFD model of the side-weir intake was developed and validated. Afterward, the analytical model, which consists of a system of three pressure drop equations for three parallel and partly imaginary streams, is formed. The local flow resistances in the analytical model are determined by the CFD model combined with RA. To equalize the flows, three solutions with (i) fix, (ii) fix in a range of flows, and (iii) variable positions of the sluice gates are analyzed.

Key words | ancillary model, CFD modeling, settling basin, side water intake, sluice gate, small hydropower plant

Miloš V. Nikolić (corresponding author)
Rade M. Karamarković
Faculty of Mechanical and Civil Engineering in Kraljevo,
University of Kragujevac,
Dositejeva 19, 36000 Kraljevo,
Serbia
E-mail: *nikolic.mi@mfkv.kg.ac.rs*

HIGHLIGHTS

- Unequal flow distribution among the chambers of a settling basin causes its malfunctioning.
- For the equalization of flows, sluice gates are used.
- A 3D CFD model of a side-weir intake is developed and validated by measurements.
- To speed up solution finding with the CFD model, an ancillary analytical model is developed.
- From three types of flow control (two with fix and one with variable gate positions), the optimal is chosen.

INTRODUCTION

Side intake structures are widely used to divert water from rivers that carry large amounts of sediment. Simple T-junctions are side intakes without damming that are suitable to divert small amounts of water. These intakes are presented and modeled in Neary & Odgaard (1993), Robinson & McGhee (1994), and Neary *et al.* (1999). To divert larger amounts of water, like in run-of-the-river hydropower plants, side intakes with damming are used. Their features, analyses, and models are presented in May *et al.* (2003) and Michelazzo *et al.* (2015).

This is an Open Access article distributed under the terms of the Creative Commons Attribution Licence (CC BY 4.0), which permits copying, adaptation and redistribution, provided the original work is properly cited (http://creativecommons.org/licenses/by/4.0/).

doi: 10.2166/hydro.2021.006

Downloaded from http://iwa.silverchair.com/jh/article-pdf/23/4/689/910515/jh0230689.pdf
by guest

If the usage of diverted water requires a limited amount of sediments with a specified size, settling basins are usually placed after the intake structures. Where the available space for intake structures is inadequate, instead of constructing long and narrow basins, multichamber settling basins are used. Their use is preferable from the operational point of view (Bishwakarma 2015).

A flow control problem at a side-weir intake with a three-chamber settling basin is addressed in the paper. Figure 1 schematically shows the intake structure of a small hydropower plant (SHPP). The intake consists of a weir, fish path with the system for ensuring environmental flow, a settling basin, and a small headpond. The settling basin consists of the common inlet and outlet zones and three settling chambers. In a settling basin, a settling chamber is the most important part, whose geometry is mainly influenced by size distribution, types, and amounts of sediment carried by the installation water flow. Settling chambers usually have trapezoidal bottom and are characterized by their length, width, depth, and water velocity (Garde *et al.* 1990; Vittal & Raghav 1997; Ranga Raju *et al.* 1999; Singh *et al.* 2008). In this settling basin, each chamber has the following features: length of 30.47 m, width of 3.30 m, depth of the transition zone of 2.20 m, whereas the settling zone has the starting depth of 3.39 m with a slope of 2.5° toward the exit. The maximal water velocity in the chamber is 0.259 m/s. At the entrance of each chamber, there is a sluice gate, which is used during the flushing of the settled sediments. Two gates are simultaneously closed during the flushing of the third chamber, whose gate is fully open.

Immediately after the commissioning of the SHPP in 2014, the malfunctioning of the settling basin was noticed. There were only small amounts of settled sediments in the third chamber. Measurements showed that at the installed flow rate of 5.65 m^3/s, the distribution of flows among the chambers is 16.00, 37.97, and 46.03% in the first, second, and third chambers, respectively. The unequal flow distribution among the chambers is identified as the main reason for the malfunctioning of the settling basin. The distribution causes that the average water velocities in the second, and especially in the third chamber (see Figure 2), exceed the maximal design velocity. During 5 years of operation, the problem decreased electricity production by 8%. A potentially more severe problem caused by nonsettled sediments is the endangerment of two turbines, each with a capacity of 1.35 MW. The turbines are parts of a combined system, which is described in detail in Karamarković *et al.* (2018).

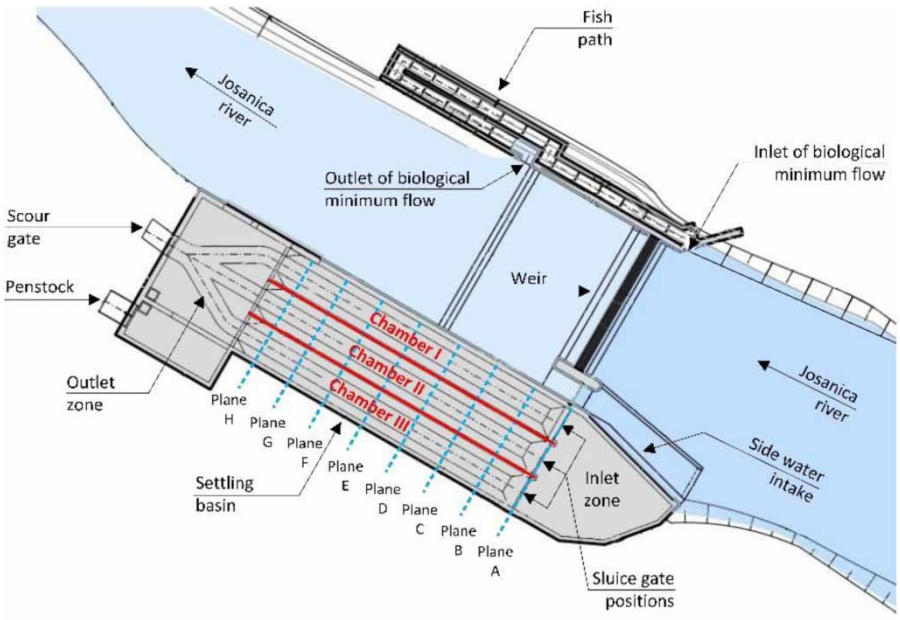

Figure 1 | Schematic of the side water intake of the SHPP.

Downloaded from http://iwa.silverchair.com/jh/article-pdf/23/4/689/910515/jh0230689.pdf
by guest

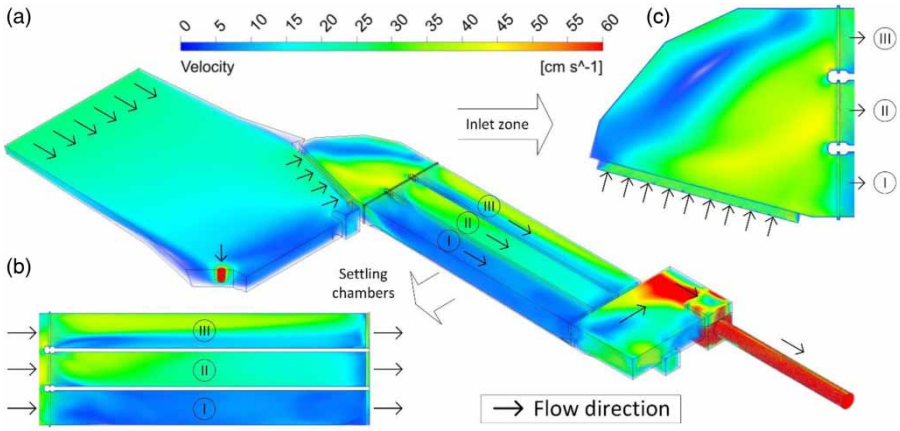

Figure 2 | The simulation results for the velocity profile inside the intake structure: (a) isometric view with flow directions, (b) velocity profiles at the upper surface of the settling chambers I, II, and III, (c) velocity profile at the upper surface of the common inlet zone.

To equalize the flows through the chambers, three solutions have been considered: (i) reconstruction according to the best practice implemented in the design of side water intakes with multichamber settling basins, (ii) the use of flow deflectors, bulkheads, etc., in the common inlet zone (Nikolić *et al.* 2021), and (iii) flow control by the use of sluice gates (Swamee 1992; Akoz *et al.* 2009; Erdbrink *et al.* 2014). Because of a large investment and long cessation of operation during the fixed subsidiary period, the reconstruction was excluded from the analysis. In the paper, the efforts are concentrated on the third method, which is the simplest, least time-consuming, and most economical for flow control through the chambers of the settling basin. To perform the task, a deep insight into the velocity field inside the intake is needed. This is achieved by the development of a 3D CFD model (Khan *et al.* 2005; Issakhanian *et al.* 2019). The model is verified based on the flow measurements that are performed according to ISO 748:2007 (ISO 748 2007). To speed up solution finding by the CFD model, an ancillary analytical model is developed. The review of additional so-called 'Data-driven models' that are used to help CFD models in solution finding is presented in detail in Solomatine & Ostfeld (2008).

METHODOLOGY

To equalize the flows through the chambers of the settling basin, three sluice gates are used (see Figures 1 and 5). To find their positions, the following methodologies were considered: (1) measurements combined with trial-and-error method (TAE), (2) measurements combined with regression analysis (RA), (3) CFD model combined with TAE, (4) CFD model combined with RA, (5) CFD model supported by a one-dimensional flow model, and (6) CFD model supported with a simple analytical model. The additional models and RA were intended to speed up the solution finding. The first four methodologies from the previous list were excluded because of the inability for proper flow measurements. Namely, the upper surface of the weir is made of reinforced concrete and has only three slits, which are used as the openings for the gates (see Figure 5). Not only do the immersed gates reduce the necessary space for the access of measuring equipment but also the measurements at these positions are not reliable (ISO 748 2007).

Figure 3 shows the procedure used for solving the problem by the fifth and sixth methodology. Initially, a 3D CFD model of the side-weir intake was developed and validated with the flow measurements according to ISO 748. The boundary conditions were adjusted so that the relative error between the flow measurements and the model predictions defers less than 8.5%. This limit is equal to the calculated measurement uncertainty, which is defined by several ISO standards (BS ISO 5168 2005; BS ISO 1088 2007; ISO 748 2007) (see Equation (3)).

The idea was to use the CFD model to find the solution with the help of an as simple as possible analytical model, which would be used as a tugboat that would navigate the

Downloaded from http://iwa.silverchair.com/jh/article-pdf/23/4/689/910515/jh0230689.pdf
by guest

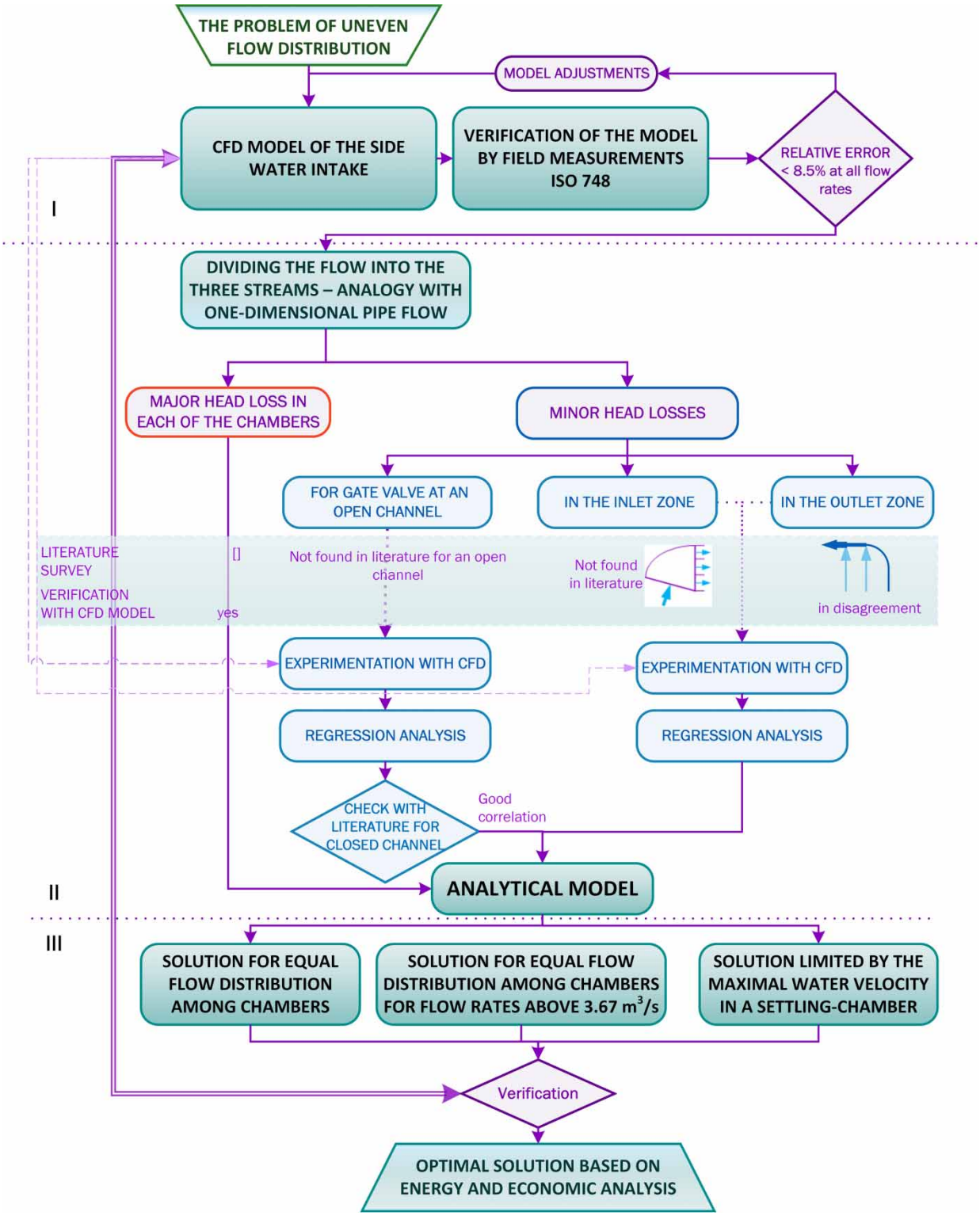

Figure 3 | The applied methodology. I, II, and III are distinctive phases during the realization.

Downloaded from http://iwa.silverchair.com/jh/article-pdf/23/4/689/910515/jh0230689.pdf
by guest

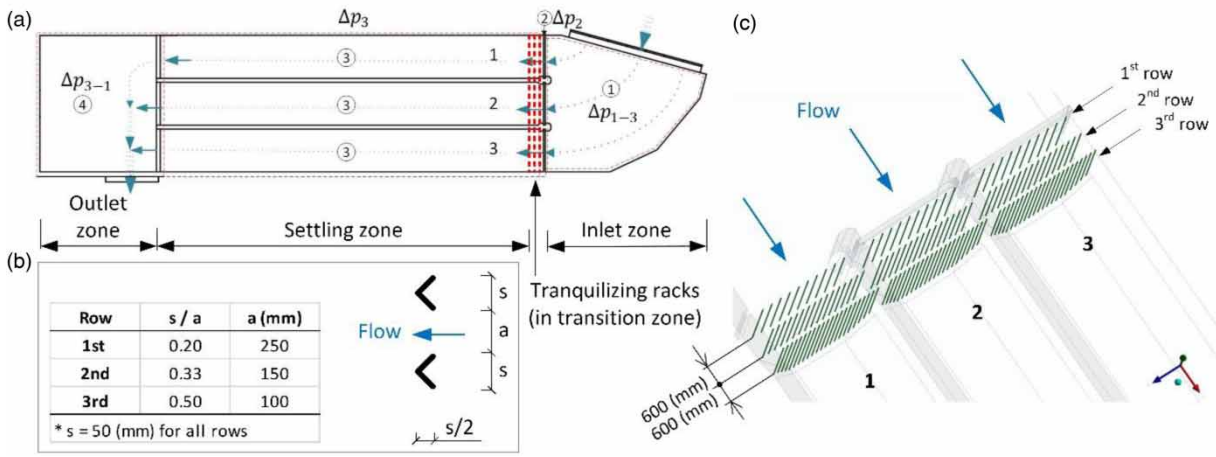

Figure 4 | Local flow resistances in the settling basin (a), the details of the tranquilizing racks (b), and their layout (c).

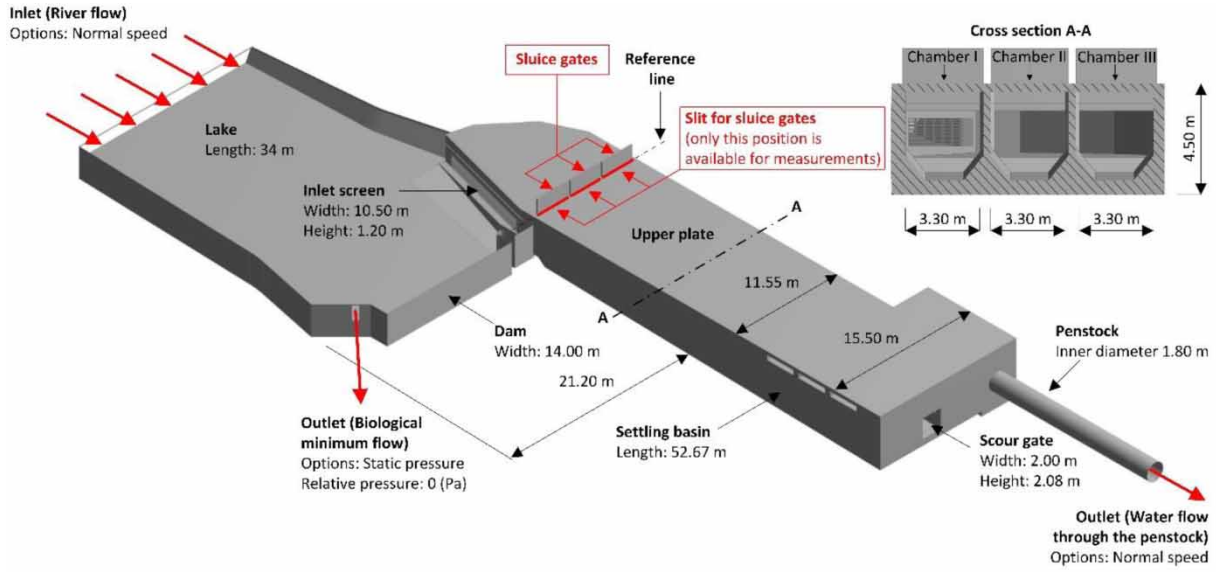

Figure 5 | Model of the side water intake.

CFD model faster toward the solution. The additional value of the analytical model would be in the dynamic flow control by the sluice gates. The development of a model analogous to a one-dimensional pipe flow model was initially tried. Its development was prevented by the inability to find minor pressure losses for a sluice gate at an open channel and for the common inlet zone (see Figures 1 and 4). In addition, the one-dimensional model for the outlet zone that consisted of two T-pipes and a 90° elbow (Idel'chik 1966) (see Figure 4(a)) showed a discrepancy with the CFD data because the real flow has three-dimensional nature. The disruption of one-dimensional flow is caused by: (i) a reinforced concrete beam that submerges the flow streams below the height of the outlet from the reservoir, which (ii) compared with the chambers has a much larger cross-sectional flow area. These were the reasons why the analogy with a one-dimensional flow model was abandoned and a bit more complex ancillary model was developed. The principle behind this analytical model is that the total flow is divided into three parallel

Downloaded from http://iwa.silverchair.com/jh/article-pdf/23/4/689/910515/jh0230689.pdf
by guest

streams (see Figure 4(a)). These streams are imaginary in the inlet and outlet zones and real in the chambers, and they have pressure drops equal to the real pressure drop. In the ancillary model, the equations for the minor losses were obtained by uniting simulation results, which were obtained by the CFD model, with RA. In this way, obtained equations for minor pressure losses in the inlet and outlet zones were verified indirectly by the verification of the analytical model. Similarly, the equation obtained for the pressure loss at the sluice gate was verified indirectly and additionally checked by the comparison with the equation for pressure drop at a gate valve installed on a closed channel (Idel'chik 1966).

It was assumed that the use of sluice gates would disturb downstream velocity profile and create backflow and vortices. Tranquilizing racks are used to prevent these disturbances by the dissipation of turbulent kinetic energy. In each chamber, the use of three rows of tranquilizing racks made of 'V' shaped bars is analyzed. Figure 4 shows the design, geometry, and positions of tranquilizing racks, whose characteristics are taken based on the model given in Paschmann (2018). For this type of rack bar, Paschmann *et al.* (2017) and Paschmann (2018) give the optimal structure configurations.

To equalize the flows, three solutions with:

1. fix positions of the sluice gates for all flow rates,
2. fix positions of the gates for flow rates above 3.67 m^3/s and the complete opening of the passages for lower flow rates, and
3. variable positions of the gates so as the average velocities in the chambers not to exceed the designed value, i.e., 0.259 m/s, are analyzed.

The CFD model and the measurements showed that below 3.67 m^3/s, the average water velocity in each chamber is lower than the designed value. These three solutions are verified, and the optimal among them is chosen by the cost–benefit analysis.

CFD MODEL VERIFICATION

To analyze the present state, a CFD model of the side water intake is used. Figure 5 shows the 3D model of the weir intake (Karamarković *et al.* 2018) with the main dimensions. At the entrance of each chamber, there is a sluice gate. The slits that allow movements of the sluice gates and the measurement of water velocities are the only opening on the reinforced concrete plate.

The model of the water intake, shown in Figure 5, is used to define a fluid domain. This domain has a total volume of 2,721.1 m^3 through which the water flows with an average temperature of 12 °C and density of 999.45 kg/m^3 (The Engineering ToolBox n.d.).

Figure 5 also shows the boundary conditions for the fluid domain. The entrance into the structure is the watercourse with the boundary type 'inlet', where the river flow is defined as an equally distributed water velocity over the cross-section. Two boundary conditions of the 'outlet' type define the exit from the structure: (i) the water flow into the penstock is defined by equal water velocities over the cross-section of the penstock at the distance of 20 m from the entrance and (ii) the water flow into the fish path, which is used to secure the environmental flow, is defined by the option 'static pressure' and by the relative pressure of 0 Pa. Because of the assumption of quasi-stationary flow, the upper water surface is modeled as the 'free slip wall', whereas all other surfaces are modeled as the 'no-slip wall'. These boundary conditions are identical as in Erdbrink *et al.* (2014), where a steady flow CFD model is used for the flow control by sluice gates, also in the case of free water surface.

The mesh consists of 2,432,345 nodes and 1,372,530 elements, each with an average volume of 1.98×10^{-4} m^3. The minimum length of a side of an element is 5 mm, whereas the maximum one is 120 mm.

The commercially available software Ansys (CFD Simulation Software, ANSYS Fluids) and its integration module CFX (ANSYS CFX: Turbomachinery CFD Simulation n.d.), according to the defined geometry, boundary conditions, and the mesh, performed the numerical simulation of water flow through the weir intake in steady-state conditions. The absolute convergence criterion that the residual is less than 1.0×10^{-4} is used for all the simulations.

Measurement procedure

As the water's surface is free (no flow under pressure), the flow through the settling basin is considered as an open-channel flow. For this reason, the flow through the settling

Downloaded from http://iwa.silverchair.com/jh/article-pdf/23/4/689/910515/jh0230689.pdf
by guest

basin is measured by means of a current meter. The measurements were conducted according to EN ISO 748: 2007 (ISO 748 2007). The standard specifies methods for determining the velocity and cross-sectional area of water flowing in open channels and for computing the discharge therefrom. The standard deals only with single measurements of the discharge.

Measurement of cross-sectional area

The cross-sectional areas of water were determined by the measuring rod BOSH GR 500 Professional (GR 500 Professional Measuring Rod, Bosch).

Figure 6 shows the plane where the measurements were performed. The widths of the chambers b-I, b-II, and b-III were measured along the reference line at the upper plate of the settling basin (see Figure 5). The depths of water in the chambers were also measured from the upper plate by measuring the depths of the chambers and the water level in relation to the reference line. The difference between these two measured values corresponds to the depth of water in the chambers h_x. The size of x is the value by which the sluice gates are constantly immersed in the water. In that way (in the plane in which the measurements were performed), the level of water in the chambers is reduced to the value $h_x - x$. The widths of the chambers are 3.20, 3.06, and 3.16 m, respectively. These values belong to the group from 3 to 5 m for which the standard (ISO 748 2007) proposes velocity measurements in the range from 13 to 16 verticals. As the measured values are very close to the lower limit of the range, 13 verticals were selected.

Velocity measurement

The standard (ISO 748 2007) defines three different methods for the determination of mean velocity in a vertical: (i) velocity distribution method, (ii) reduced point method, and (iii) integration method. Based on the site specificities, the required number of measuring verticals $\sum n = 39$ and measuring equipment (GR 500 Professional Measuring Rod, Bosch; JDC Electronic SA – Flowatch n.d.), the reduced point method was selected. This is the most often used method because it requires less time compared with the other two. It is based on the theoretical velocity profile. This method allows determining the mean velocity in a vertical by measuring in just one or up to six points. To increase the accuracy of the mean velocity in a vertical, the velocities are measured in the maximum allowed number of points for this method (six). The velocities are measured in each vertical at 0.2, 0.4, 0.6, and 0.8 of the water depths ($h_x - x$) below the surface of the water, and as close as possible to the water surface and at the bottom of the channel. The mean velocity in a vertical is calculated as follows (ISO 748 2007):

$$\bar{v} = 0.1(v_{\text{surface}} + 2v_{0.2} + 2v_{0.4} + 2v_{0.6} + 2v_{0.8} + v_{\text{bed}}), \quad (1)$$

where v_{surface} and v_{bed} are velocities close to the surface of the water and the bottom of the channel, and $v_{0.2}$, $v_{0.4}$, $v_{0.6}$, and $v_{0.8}$ are velocities that correspond to the

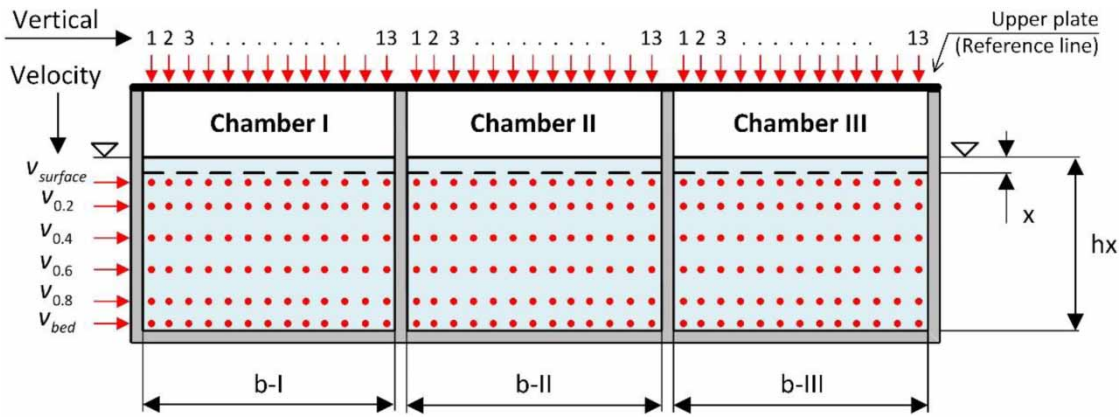

Figure 6 | A schematic view of the measurement plane.

Downloaded from http://iwa.silverchair.com/jh/article-pdf/23/4/689/910515/jh0230689.pdf
by guest

heights of 0.2, 0.4, 0.6, and 0.8 from the water depth ($h_x - x$) under the surface, respectively.

Figure 6 also shows the velocity measuring plan, which is formed based on the number of verticals and the number of measuring points per one vertical defined by Equation (1). The spots in Figure 6 represent the measuring points – there are 78 in each of the three chambers, i.e., 234 in the measuring plane. The ISO standard (ISO 748 2007) defines that the exposure time of the current meter at each measuring point must be 0.5, 1, 2, or 3 min. In the paper, considering the large number of measuring points, the least allowed exposure time of 0.5 min was selected. The necessary condition for the successful measurement of the velocity field is to maintain a constant flow through the SHPPs, i.e., through the examined settling basin.

Computation of discharge

The mid-section method (Herschy 2009) as a part of arithmetic methods is used for the computation of discharge. In each of the three chambers, for the defined number of verticals $n = 13$, the total discharge is calculated as follows:

$$Q = \sum_{n=1}^{13} \left[\bar{v}_n \cdot h_n \cdot \left(\frac{b_{n+1} - b_{n-1}}{2} \right) \right] \tag{2}$$

where $\bar{v}_n$ is the mean vertical velocity in the observed segment defined by Equation (1), h_n is the depth of the vertical in the observed segment, and b_{n-1} and b_{n+1} are the positions of adjacent verticals measured from the fixed reference point.

Uncertainties in flow measurement

The international standards (BS ISO 5168 2005; BS ISO 1088 2007) were used to calculate the relative combined standard uncertainty of the measurement:

$$u(Q_c) = \left[u_n^2 + u_s^2 + \left(\frac{1}{n} \right) \cdot \left(u_b^2 + u_d^2 + u_p^2 + \left(\frac{1}{m} \right) \cdot (u_c^2 + u_e^2) \right) \right]^{1/2}, \tag{3}$$

where u_b and u_d are the relative standard uncertainties in the width and depth, u_p is the uncertainty in the mean velocity, $\bar{v}_i$ due to the limited number of depths at which velocity measurements are made at the vertical, u_n is the uncertainty due to the limited number of verticals, m is the number of depths in the vertical at which velocity measurements are made, n is the number of verticals, u_c is the uncertainty in the velocity at a particular measuring point in the vertical due to the lack of repeatability of the current meter, u_e is the uncertainty in point velocity at a particular depth in the vertical due to velocity fluctuations (pulsations) in the stream during the exposure time of the current meter, and u_s is the uncertainty due to variable responsiveness of the current meter (u_{cm}), width measurement instrument (u_{bm}), and depth sounding instrument (u_{ds}).

Verification of the model

The model was verified by three particular measurement sessions at different rates of discharge, which were constant and approximately 100, 72, and 52% of the installed flow. The velocity measurement plan, which is schematically shown in Figure 6, was used for these measurements. The exposure time of the measuring device at each point was 30 s. In the remainder, only the detailed measuring results at the installed flow rate are presented.

Figure 7 shows the comparative results of mean velocities in the verticals from 1 (V-1) to 13 (V-13) in all three chambers. The mean velocities in the verticals were calculated using Equation (1) based on the measured and simulated values. The width of the chamber and the distances between the verticals are defined according to the Standard (ISO 748 2007).

Based on the calculated mean velocities in the verticals and the known widths and depths of the water in the chambers, flow rates through the settling basin were calculated. The uncertainty in the flow measurement is 8.48% with a confidence level of 95% and was calculated by Equation (3).

Table 1 shows the relative errors of discrepancies in the chambers for the flow rates obtained by the CFD model in relation to the flow rates obtained by the measurements. The errors for all measurements in all three chambers are less than the calculated measurement uncertainty of 8.48% so that the results of the CFD model can be considered to

Downloaded from http://iwa.silverchair.com/jh/article-pdf/23/4/689/910515/jh0230689.pdf
by guest

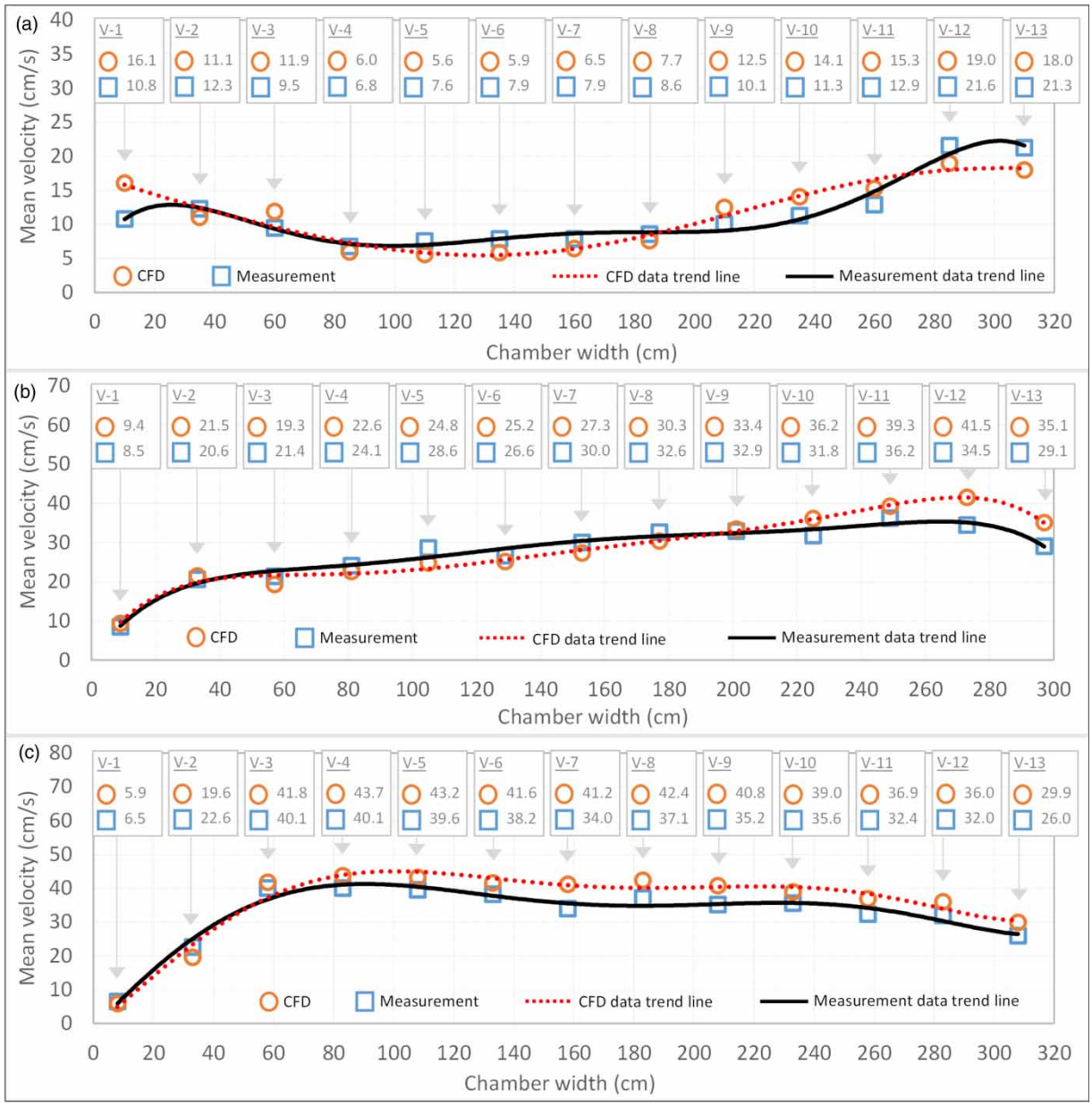

Figure 7 | Comparative results of mean velocities in: (a) chamber I, (b) chamber II, and (c) chamber III at the installed flow rate (see Figures 1 and 2).

represent a realistic image of the flow through the chambers of the settling basin.

ANCILLARY MODEL

To speed up the CFD model, an ancillary analytical model is developed and is used for the dynamic flow control by the sluice gates. The inlet section of the model is placed just downstream of the inlet screen, whereas the outlet section is placed at the exit of the common outlet zone (see Figures 1 and 4(a)). The screen does not influence the flow distribution in the settling basin because of its design. This is verified by the CFD model and can be seen in Figure 2.

To find the positions of the sluice gates, the total flow is divided into three parallel streams from the inlet to the

Downloaded from http://iwa.silverchair.com/jh/article-pdf/23/4/689/910515/jh0230689.pdf
by guest

Table 1 | Errors of flow rates for all three particular measurement sessions

Measurement		Chamber I	Chamber II	Chamber III
1	Measured flow (l/s)	846	2,007	2,433
	Simulated flow (l/s)	791	1,906	2,553
	Relative error (%)	6.50	5.03	4.93
2	Measured flow (l/s)	666	1,415	1,826
	Simulated flow (l/s)	610	1,355	1,841
	Relative error (%)	8.41	4.24	0.82
3	Measured flow (l/s)	472	974	1,268
	Simulated flow (l/s)	457	1,016	1,370
	Relative error (%)	3.18	4.31	8.04

outlet sections (see Figure 4(a)). These streams are imaginary in the inlet and outlet sections and real in the chambers. As the streams are parallel, their pressure drops are equal to the total pressure drop between the inlet and outlet sections, i.e., $\Delta p_1 = \Delta p_2 = \Delta p_3$, and are calculated by:

$$\text{Streamline 1: } \Delta p_1 = (\Delta p_{1-3})_1 + (\Delta p_{sg})_1 + (\Delta p_l)_1 + (\Delta p_{3-1})_1, \quad (4)$$

$$\text{Streamline 2: } \Delta p_2 = (\Delta p_{1-3})_2 + (\Delta p_{sg})_2 + (\Delta p_l)_2 + (\Delta p_{3-1})_2, \text{ and} \quad (5)$$

$$\text{Streamline 3: } \Delta p_3 = (\Delta p_{1-3})_3 + (\Delta p_{sg})_3 + (\Delta p_l)_3 + (\Delta p_{3-1})_3. \quad (6)$$

In Equations (4)–(6) for the i-th streamline (subscript $i = 1 \div 3$), $(\Delta p_{1-3})_i$ and $(\Delta p_{3-1})_i$ in (Pa) are the pressure drops made by imaginary streams in the inlet and outlet sections, $(\Delta p_{sg})_i$ in (Pa) are the pressure drops at the sluice gates, and $(\Delta p_l)_i$ in (Pa) are the pressure drops due to friction in the settling chambers. The friction losses are calculated by the Darcy–Weisbach equation (Anagnostopoulos & Papantonis 2007), whereas the other pressure drops are calculated using minor loss coefficients, whose determinations are explained in the following sections.

Dynamic pressure loss coefficient for an open channel sluice gate

The idea to solve the problem of unequal flow distribution through the chambers of the settling basin is to find the right positions for sluice gates at the entrances of the second and third chambers (see Figure 5). The dynamic pressure loss coefficient for a closed channel gate valve can be found, e.g., in Idel'chik (1966). However, the adequate equation for an open channel sluice gate has not been found. The impossibility to measure pressure drop of the installed sluice gates instigated CFD simulations. Figure 8 shows the modeling details. Flow rates and geometry are taken for the examined case. The distances of five hydraulic diameters, upstream and downstream of the sluice gate are taken to stabilize the flow. In total, 100 simulations were done for 10 flow rates (in the range $0.565 \div 5.65$ m^3/s with the step 0.565 m^3/s) and for each flow rate for 10 positions of the gate ($0.1\text{ h} \div \text{h}$, step 0.1 h). The least-squares regression model was used to find the function that describes the simulation results (Birkes & Dodge 1993; Draper & Smith 1998). The regression model (Equation (7)) consists of five predictor terms (variables) and six unknown coefficients. In the model, the response variable is the pressure drop, whereas predictor variables are the relative openness of the sluice gate and the square of the average velocity multiplied by the series of power terms of the relative openness raised to the powers of 0, 1/2, 1, 3/2, and 2. The regression model describes well the simulation results as R^2 is 0.999996 (Draper & Smith 1998). Table 2 shows the regression coefficients and the corresponding p-values in the t-test, which were used for their evaluation (Birkes & Dodge 1993). As the t-tests are far enough from 0 and the p-values are substantially below 0.05, the regression coefficients are significant (Birkes & Dodge 1993).

$$\Delta p = C_0 + C_1 \cdot \sqrt{\frac{h_x - x}{h_x}} + \left[C_2 + C_3 \cdot \left(\frac{h_x}{h_x - x} \right)^2 + C_4 \cdot \left(\frac{h_x}{h_x - x} \right)^{\frac{3}{2}} + C_5 \cdot \frac{h_x}{h_x - x} \right] \cdot \frac{\rho \cdot w^2}{2}, \quad (7)$$

where C_0, C_1, C_2, C_3, C_4, and C_5 are regression constants given in Table 2, h_x (m) is the depth of the channel, x (m) is the depth to which the gate is immersed into water, $\rho = 999.45$ (kg/m^3) is the average water density during the year, at 12°C (The Engineering ToolBox n.d.), and w (m/s) is the average water velocity at the inlet.

Downloaded from http://iwa.silverchair.com/jh/article-pdf/23/4/689/910515/jh0230689.pdf
by guest

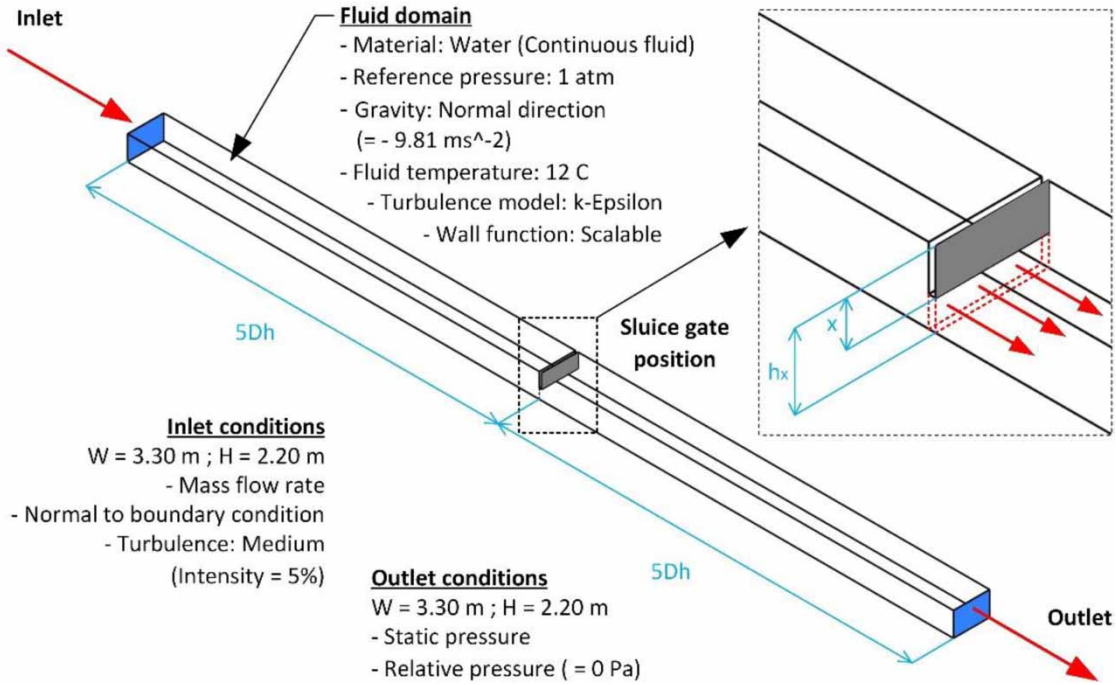

Figure 8 | Isometric view of the CFD model together with the modeling details that are used to simulate the water flow through the sluice gate at an open channel.

Table 2 | Regression constants, *t*-stat, and *p*-value for Equation (7)

	C_0	C_1	C_2	C_3	C_4	C_5
Regression constants	1.378	−1.528	2.572	1.082	5.569	−9.232
t-stat	2.069	−2.451	20.686	11.879	15.723	−24.236
p-value	0.043	0.017	<0.01	<0.01	<0.01	<0.01

Table 3 shows the comparison of minor loss coefficients obtained by Equation (7) and by the equation taken from Idel'chik (1966) for closed channel gate valve depending on the relative openness of the gates. In the range from 20 to 80% of the nominal flow rate, these expressions have a good correlation. Compared with the closed channel, the open channel sluice gate produces a slightly larger pressure drop because of the free movement of the water surface in front of the gate.

Common inlet zone

From the common inlet zone, the diverted flow exits divided into three streams (see Figures 1, 2, and 4a), which enter the chambers of the settling basin. Because of the unique geometry of the zone, the minor pressure loss coefficient was not found in the literature. The same methodology as in the previous case is applied (CFD simulations + RA). Figure 9 shows the 3D model with simulation details,

Table 3 | The comparison of minor loss coefficients obtained by Equation (7) for an open channel and by equation taken from Idel'chik (1966) for closed channel gate valve depending on the relative openness of the gates $(h_x - x)/h_x$

$(h_x - x)/h_x$	0	0.1	0.2	0.3	0.4	0.5	0.6	0.7	0.8	0.9	1
Idel'chik (1966)	∞	193	44.5	17.8	8.12	4.02	2.08	0.95	0.39	0.09	0
This study	–	165.94	45.36	17.71	8.28	4.19	2.18	1.10	0.51	0.17	–

Downloaded from http://iwa.silverchair.com/jh/article-pdf/23/4/689/910515/jh0230689.pdf
by guest

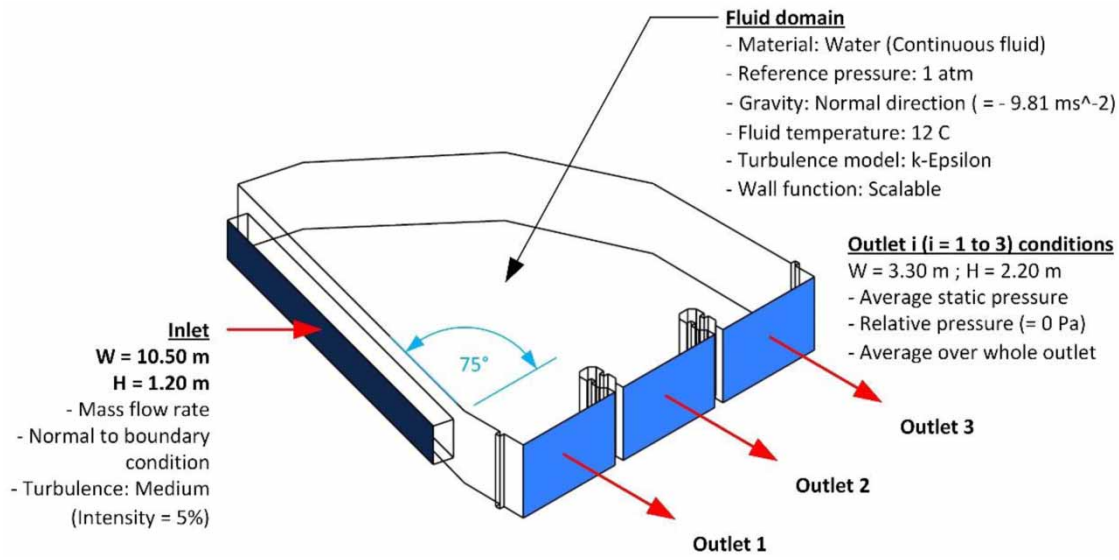

Figure 9 | Isometric view of the CFD model together with the modeling details that are used to simulate the flow through the inlet zone.

whereas Figure 10 depicts simulation results for the two characteristic flow rates. The simulations were done in the range of flows from $0.65Q_{in}$ to Q_{in}, with the step $0.05Q_{in}$ for two cases: (1) with free discharge from the zone and (2) with the condition that exit flows are equal. The first case matches the present conditions, whereas the second

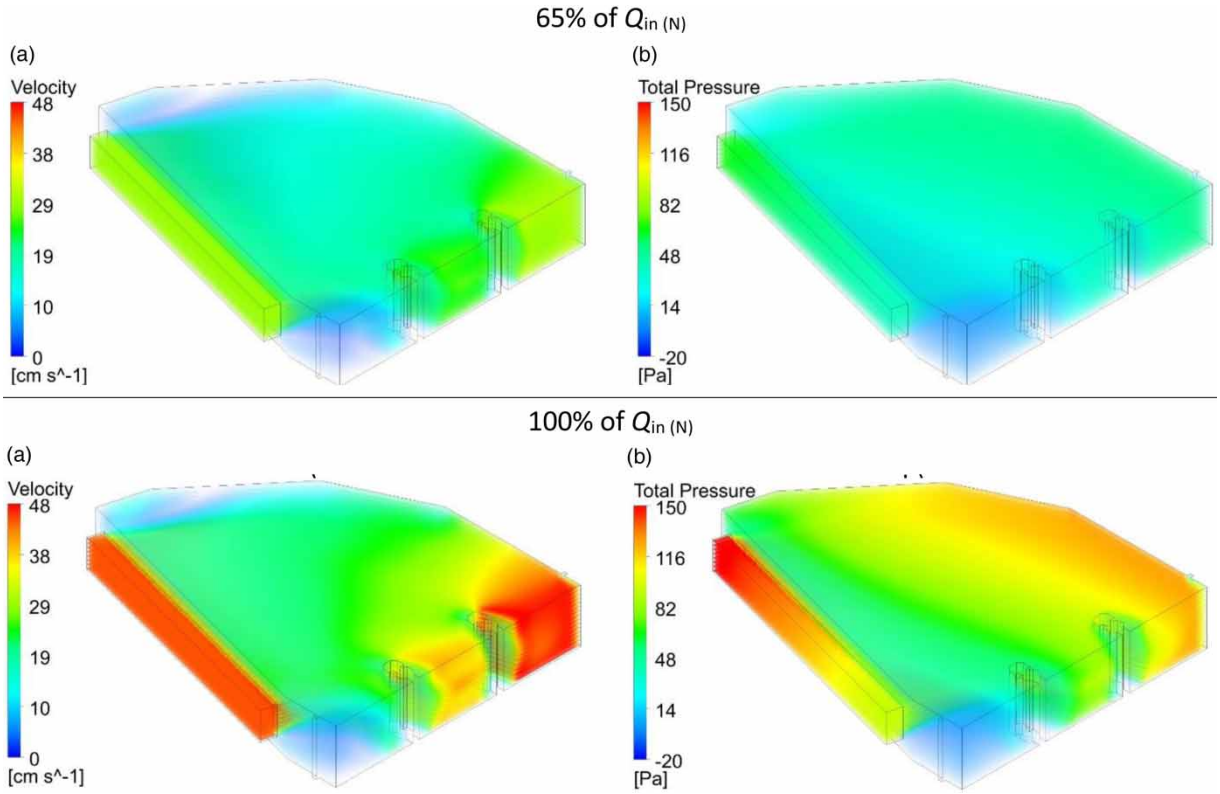

Figure 10 | CFD simulations for the two characteristic flows through the inlet zone: (a) velocity distribution and (b) pressure distribution.

Downloaded from http://iwa.silverchair.com/jh/article-pdf/23/4/689/910515/jh0230689.pdf
by guest

matches the desired conditions. In each case, there were eight simulations. The regression model consists of four predictor variables and five regression constants. Equation (8) describes well the simulation results as $R^2 > 0.999987$. The three predictor variables are the square differences of the average velocities at the entrance and at the three corresponding exits each divided by the appropriate radius of the curvature, and the fourth is the water flow rate at the entrance. Table 4 shows the values and that the regression coefficients are significant as their p-values are below 0.5 and the *t*-tests enough above zero, which is in agreement with Birkes & Dodge (1993).

$$\Delta p_k = C_0 + C_1 \cdot Q_{\text{in}} + \sum_{i=1}^{3} C_{i+1} \cdot \frac{(\bar{w}_{\text{in}} - \bar{w}_i)^2}{R_i}, \tag{8}$$

where $k = 1 \div 3$ is the number of the chamber, Q_{in} (m^3/s) is the total flow rate at the entrance, $\bar{w}_{\text{in}}$ (m/s) is the average water velocity at the entrance to the zone, $\bar{w}_i$ (m/s) is the average water velocity entering the *i*th chamber, R_i (m) is the radius that connects the middles of the *i*th third (from right to left) of the inlet section and the *i*th chamber, and C_i ($i = 0 \div 4$) are regression constants that are given in Table 4.

Outlet zone

Three separated flows from the settling basin enter, and the total flow laterally exits the outlet zone (see Figures 4(a) and 11). As it was already explained, this resistance could not be described by a one-dimensional flow analogy. Therefore, CFD simulations were done as in the previous cases. In these simulations, the flow rates were varied in the range from $0.65Q_{\text{in}}$ to Q_{in}, with the step $0.05Q_{\text{in}}$ for the two similar cases as in the inlet zone: (1) for free inflow into the zone and (2) for equal inflows from the chambers into the outlet zone. The first case matches the present, whereas the second matches the desired conditions. Figure 12 shows simulation results for the two characteristic flows. The assumed regression model (Equation (9)) describes well the simulation results as $R^2 > 0.999986$. It is analogous to Equation (8), which is used to describe the simulation results for the common inlet zone. In Equation (9), the three predictor variables are assumed to be the squared differences of water velocities at the exit and the entrance from each chamber divided by the corresponding distance between the middle of each entrance and the exit from the zone. The fourth predictive variable is the total flow at the exit of the zone. Table 5 shows the values and that the regression coefficients are significant as their p-values are below 0.5 and the *t*-tests enough above zero, which is in agreement with Birkes & Dodge (1993).

$$\Delta p = C_0 + C_1 \cdot Q_{\text{in}} + C_2 \cdot \frac{(w_{\text{out}} - w_1)^2}{b_1} + C_3 \cdot \frac{(w_{\text{out}} - w_2)^2}{b_2} + C_4 \cdot \frac{(w_{\text{out}} - w_3)^2}{b_3} \tag{9}$$

where $\bar{w}_{\text{out}}$ (m/s) is the average water velocity at the outlet of the zone, $\bar{w}_i$ (m/s) is the average water velocity entering the outlet zone from the *i*th chamber, and C_i ($i = 0 \div 4$) are regression constants that are given in Table 5.

Table 4 | Regression constants that are used in Equation (8) with *t*-stats and *p*-values for three streams

Chamber		C_0	C_1	C_2	C_3	C_4
I	Regression constants	−2.914	1.277	1,674.310	2,219.056	15,894.092
	t-stat	−4.356	2.335	3.026	4.275	3.543
	p-value	<0.01	0.044	0.014	<0.01	<0.01
II	Regression constants	−1.004	0.466	1,060.100	1,674.298	1,171.772
	t-stat	3.377	3.946	5.484	5.923	2.563
	p-value	<0.01	<0.01	<0.01	<0.01	0.030
III	Regression constants	0.611	−0.282	608.064	222.123	−4,001.306
	t-stat	2.789	−2.851	6.909	3.373	−2.441
	p-value	0.021	0.019	<0.01	<0.01	0.037

Downloaded from http://iwa.silverchair.com/jh/article-pdf/23/4/689/910515/jh0230689.pdf
by guest

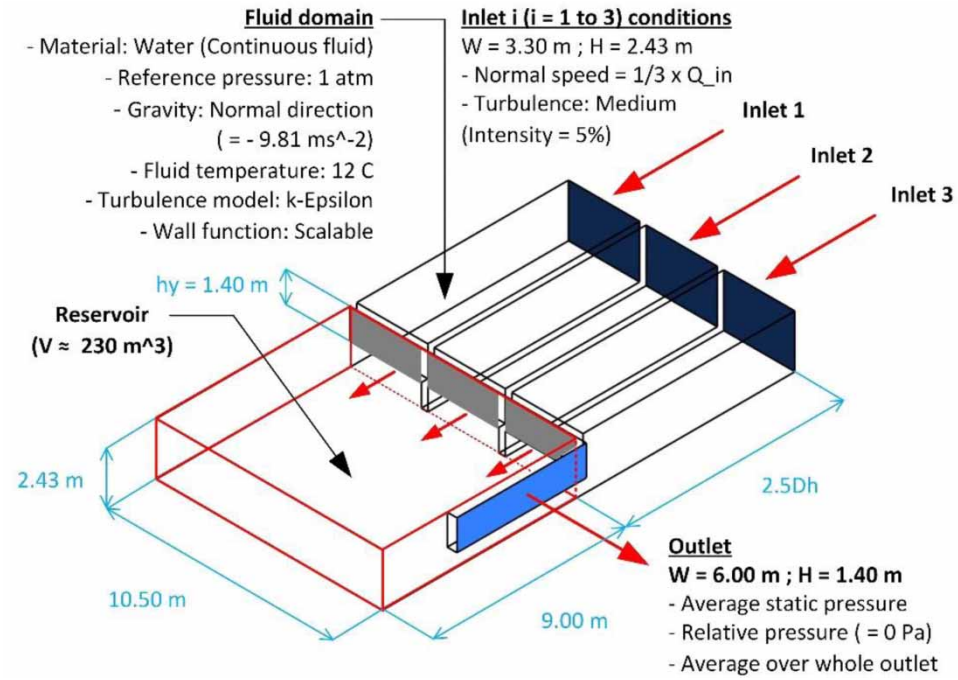

Figure 11 | Isometric view of the CFD model together with the modeling details that are used to simulate the flow through the outlet zone.

RESULTS

Figure 13 illustrates the results obtained by solving the analytical model for sluice gate positions. These are obtained for three types of flow control: (i) fix positions for all flow rates, (ii) fix positions for flow rates above 3.67 m^3/s, and (iii) variable positions of the gates so that the average water velocities do not exceed the designed value for the settling chambers, i.e., 0.259 m/s.

Table 6 and Figure 14 show the verification of previously mentioned results by the CFD model. Table 6 shows that the usage of sluice gates equalizes the flow rates and average velocities among the chambers. However, their usage impacts the downstream velocity profiles, which are shown in Figure 14 for all the chambers in eight equidistant sections at the installed flow rate. The flow disturbances propagate approximately up to the middle of the third and up to the first third of the second chamber. The highest velocities are at the bottom and are shifted toward the outer curve of the common inlet zone. The positive in this velocity profile is that the highest velocities are at the bottom, where the settling path is the shortest.

Figure 15 shows the propagation of velocity disturbances in the third chamber, which is critical because of the largest closeness of the sluice gate. The problem is accentuated at the highest flow rates and could be mitigated using tranquilizing racks. The racks are used to create a well-distributed flow in the chambers by the dissipation of turbulent kinetic energy. Figure 4 shows the features of the analyzed racks made of 'V' shaped bars that are used to mitigate turbulent flows in all three chambers. Figures 14 and 15 show CFD simulations, which examine the usage of tranquilizing racks just downstream of the gates. Their use reduces the zone of disturbance and maximal velocities and completely stops backflow and vortices. Figure 15 shows the development of secondary flow near the water surfaces behind the tranquilizing rack. This flow has a minor influence on the settling process.

Table 7 shows the influence of the three analyzed flow control solutions on electricity production. These are calculated based on the flow duration curve (given in Supplementary Material, Appendix A) and pressure losses, which are shown in Figure 16 and obtained by Equations (4)–(6). Figure 16 also shows the equations for pressure losses through the weir

Downloaded from http://iwa.silverchair.com/jh/article-pdf/23/4/689/910515/jh0230689.pdf
by guest

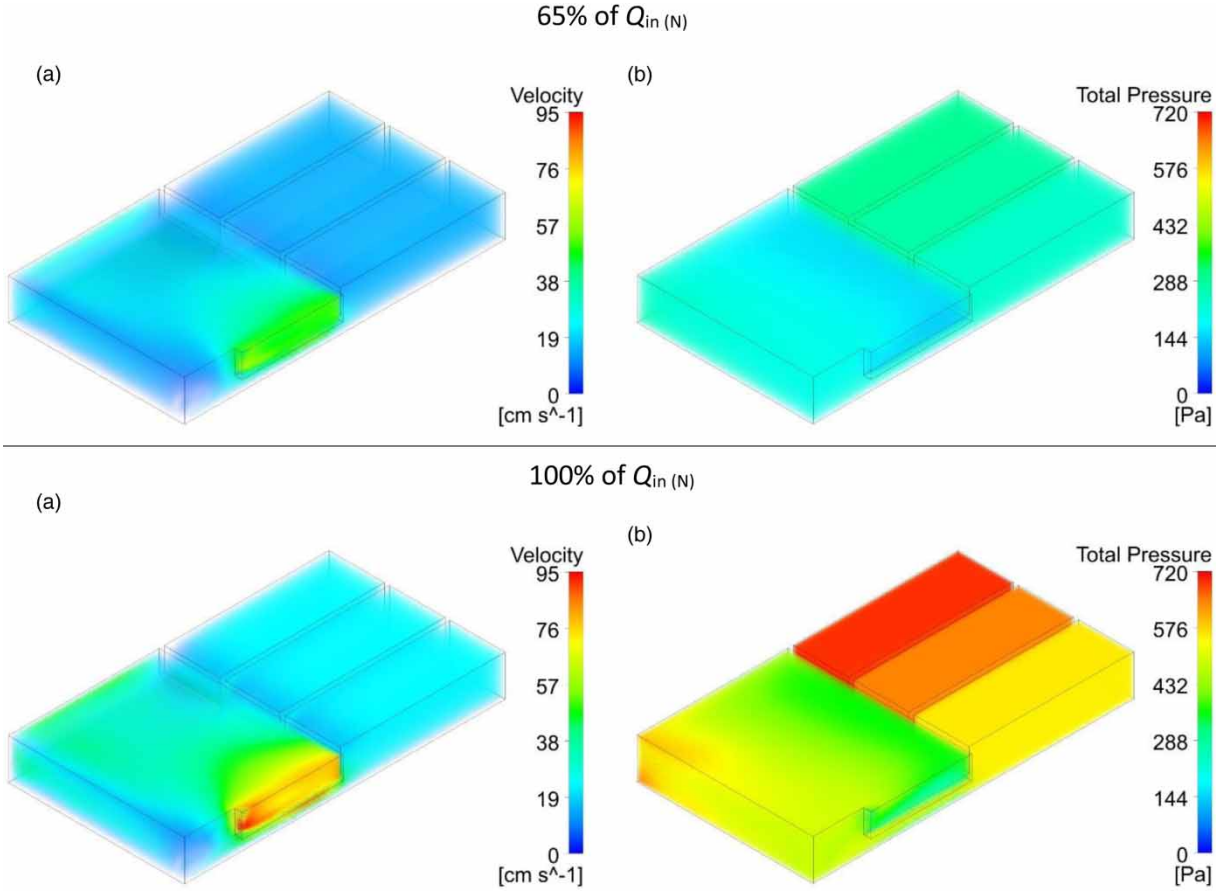

Figure 12 | CFD simulations for the two characteristic flows through the outlet zone: (a) velocity distribution and (b) pressure distribution.

Table 5 | Regression constants that are used in Equation (9) with *t*-stats and p-values for three streams

Chamber		C_0	C_1	C_2	C_3	C_4
I	Regression constants	−9.196	3.890	109,321.897	−230,394.189	55,460.678
	t-stat	−3.042	2.510	3.257	−2.785	2.370
	p-value	0.014	0.033	<0.01	0.021	0.042
II	Regression constants	−8.172	3.816	141,292.471	−273,628.086	62,653.488
	t-stat	2.592	2.904	2.559	−3.976	3.015
	p-value	0.029	0.017	0.031	<0.01	0.015
III	Regression constants	−11.892	5.481	142,391.135	−261,121.114	57,724.004
	t-stat	−2.835	2.938	2.329	−3.972	2.941
	p-value	0.019	0.016	0.045	<0.01	0.016

depending on the flow rate and the type of flow control. Compared with the solutions that have fix positions of sluice gates, the dynamic control causes smaller pressure losses. However, regardless of the type, the flow control causes the pressure drop that is negligible (221 Pa, see Figure 16) if compared with the total pressure drop at the SHPP (82,196 Pa) (Karamarković *et al.* 2016, 2018). The applied type of flow control is almost irrelevant to the electricity production. From this fact, it is obvious that economic analysis favors simple solutions that have fix sluice gate positions.

Downloaded from http://iwa.silverchair.com/jh/article-pdf/23/4/689/910515/jh0230689.pdf
by guest

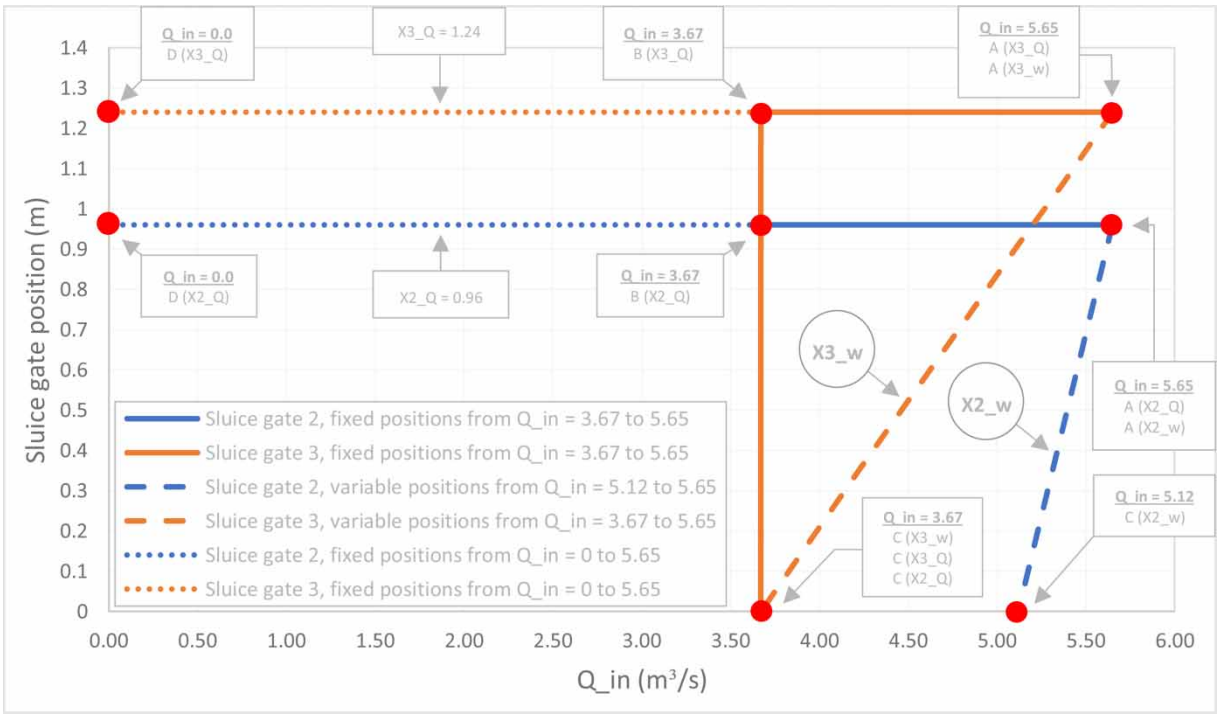

Figure 13 | The positions of the sluice gates in the second and third chambers depending on the type of flow control.

Table 6 | The flow distribution through the settling chambers depending on the regulation method and the relative flow rate (100% corresponds to the installed flow)

		Before flow regulation		Equal flow method		Maximum velocity limitation method	
Q_{in} (%)	Chamber	Relative flow distribution (%)	Mean velocity (cm/s)	Relative flow distribution (%)	Mean velocity (cm/s)	Relative flow distribution (%)	Mean velocity (cm/s)
100	I	11.70	9.1	32.92	17.2	32.92	17.2
	II	38.82	30.2	33.61	17.5	33.61	17.5
	III	49.48	38.5	33.48	17.5	33.48	17.5
95	I	11.95	8.2	32.93	16.3	27.29	13.5
	II	38.82	27.2	33.60	16.7	36.68	18.2
	III	49.43	34.7	33.47	16.6	36.03	17.9
85	I	13.65	8.5	32.97	14.6	21.46	9.5
	II	37.33	23.2	33.59	14.9	37.77	16.8
	III	49.02	30.5	33.43	14.8	40.77	18.1
75	I	13.70	7.5	33.03	12.9	14.28	5.6
	II	37.35	20.3	33.58	13.1	39.47	15.4
	III	48.95	26.7	33.39	13.1	46.25	18.1
65	I	13.73	6.9	33.06	11.2	12.53	4.3
	II	37.35	18.9	33.60	11.4	38.08	12.9
	III	48.91	24.7	33.34	11.3	49.40	16.8

CONCLUSIONS

The main conclusions regarding the problem are as follows:

1. The existing sluice gates can be used to control the flows through the settling chambers. Their application equalizes flow rates and average velocities among the

Downloaded from http://iwa.silverchair.com/jh/article-pdf/23/4/689/910515/jh0230689.pdf
by guest

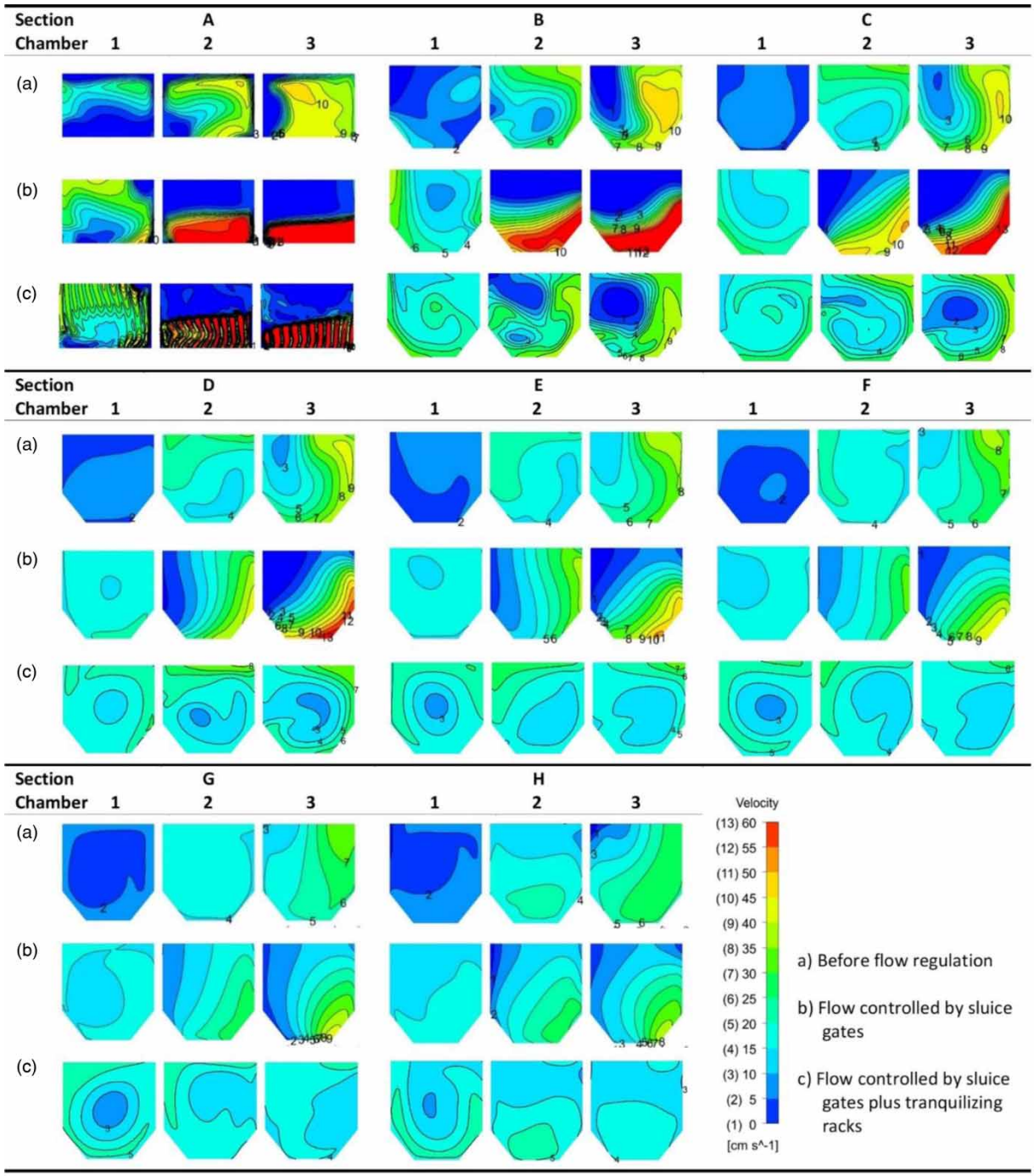

Figure 14 | Velocity profiles in eight sections of the settling basin for the nominal flow rate depending on the chamber, the usage of sluice gates for flow control, and the usage of tranquilizing racks.

chambers but influences the downstream velocity profiles. To create a well-distributed flow without vortices in the chambers, tranquilizing racks should be used just after the gates. In the examined case, their usage completely stops backflow and vortices and reduces maximal velocities in the chambers.

2. All three analyzed solutions, two with fix and one with variable positions of the sluice gates, are applicable and

Downloaded from http://iwa.silverchair.com/jh/article-pdf/23/4/689/910515/jh0230689.pdf
by guest

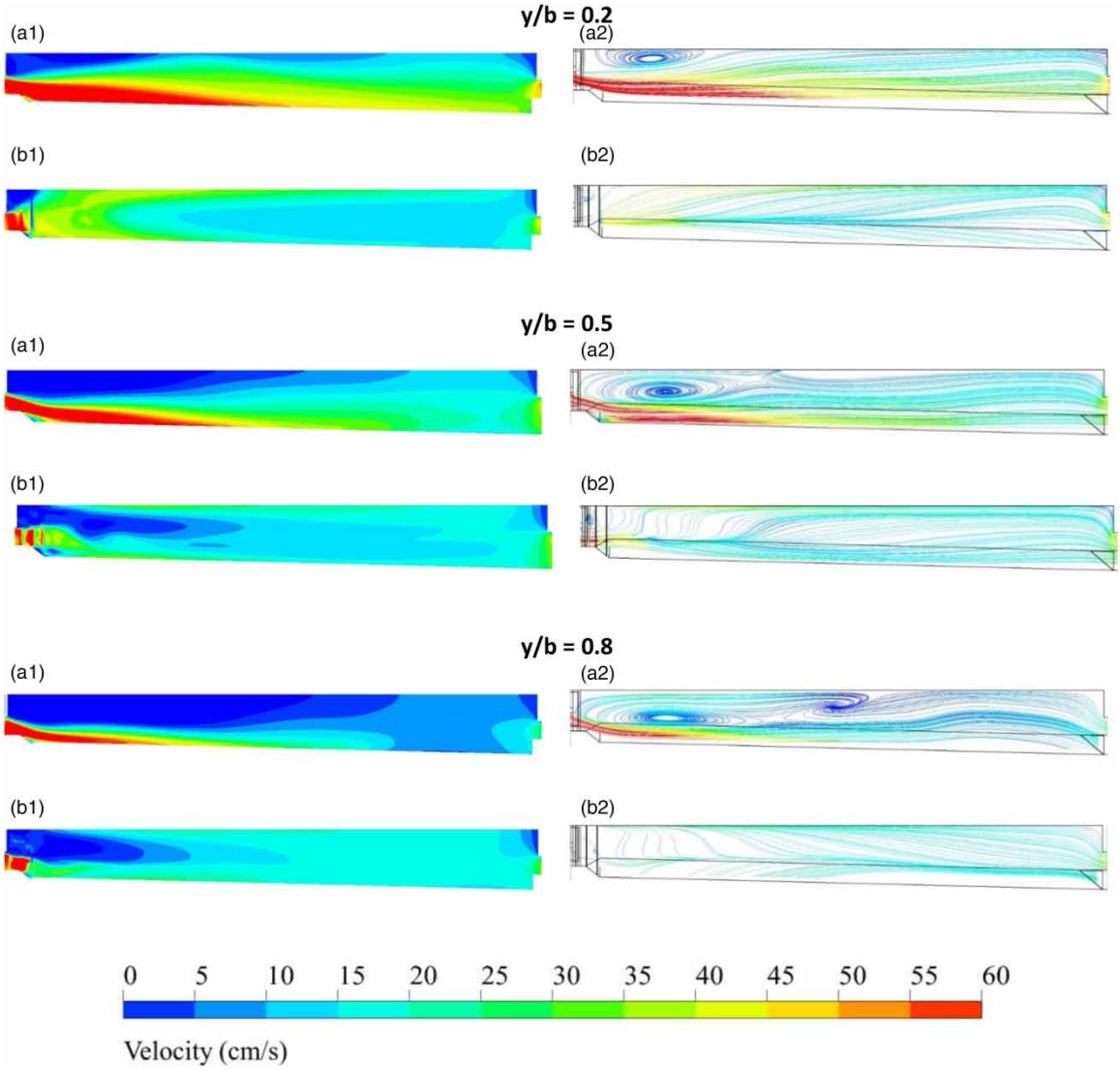

Figure 15 | The impact of the tranquilizing rack on the velocity profiles in the third settling chamber at the installed flow. In the figure, *y/b* is the relative distance from the right edge (downstream) of the chamber, (a1) velocity profile and (a2) streamlines in the section without the tranquilizing rack, whereas (b1) and (b2) are the same as (a1) and (a2) but with the tranquilizing rack.

Table 7 | The impact of the type of flow control on the electricity production by the SHPP

Type of flow control	Electricity production (MWh)	Difference (MWh)	Relative difference (%)
Wthout control (present case)	4,401.35		
Variable gate positions ($Q_{in} = 3.67$–5.65 m^3/s)	4,400.30	1.05	0.0239
Fix positions ($Q_{in} = 3.67$–5.65 m^3/s)	4,399.85	1.50	0.0341
Fix positions ($Q_{in} = 0.00$–5.65 m^3/s)	4,399.60	1.75	0.0398

all have a small impact on electricity production. Consequently, the cheapest solution that uses permanent positions of the sluice gates is preferable.

3. The geometrical and flow symmetry eliminates the need for flow control in multichamber settling basins.
4. Compared with the pressure losses in the inlet and outlet zones of a multichamber settling basin, the losses in the settling chambers are much smaller. Therefore, in this type of basin, the different widths could not be used to equalize flows through the settling chambers.

Downloaded from http://iwa.silverchair.com/jh/article-pdf/23/4/689/910515/jh0230689.pdf
by guest

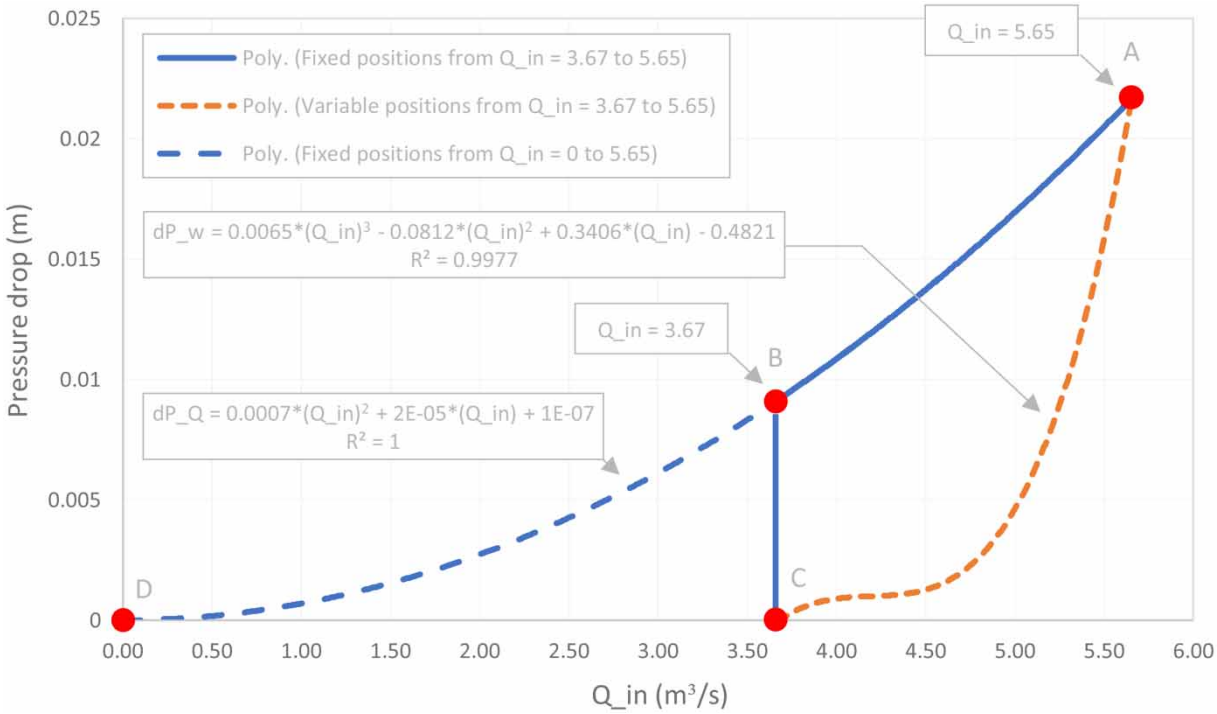

Figure 16 | The pressure drop in the settling basin depending on the type of flow control.

The main conclusions regarding the problem and the applied methodology for its solving are as follows:

- If the intake design enables reliable flow measurements, their combination with RA is the easiest and the least time-consuming way to solve this kind of problem.
- If verified CFD models exist for similar flow control problems, the solution finding could be speeded up by combining the model with RA.
- In flow control problems, where proper measurements are not possible, as in the presented case, the solution finding with the CFD model could be speeded up using a simple analytical or 'data-driven' model.
- Equation (7) can be used to calculate pressure drops at open-channel sluice gates.

ACKNOWLEDGEMENTS

This research was supported by the Ministry of Education, Science and Technological Development of the Republic of Serbia (Grant No. 451-03-9/2021-14/200108).

DATA AVAILABILITY STATEMENT

All relevant data are included in the paper or its Supplementary Information.

REFERENCES

Akoz, M. S., Kirkgoz, M. S. & Oner, A. A. 2009 Experimental and numerical modeling of a sluice gate flow. *Journal of Hydraulic Research* **47** (2), 167–176. https://doi.org/10.3826/jhr.2009.3349.

Anagnostopoulos, J. S. & Papantonis, D. E. 2007 Optimal sizing of a run-of-river small hydropower plant. *Energy Conversion and Management* **48** (10), 2663–2670. https://doi.org/10.1016/j.enconman.2007.04.016.

ANSYS CFX: Turbomachinery CFD Simulation n.d. Available from: https://www.ansys.com/products/fluids/ansys-cfx (accessed 13 December 2020).

Birkes, D. & Dodge, Y. 1993 *Alternative Methods of Regression*. John Wiley & Sons, New York.

Bishwakarma, M. B. 2015 Settling basin design criteria and trap efficiency computation methods. *Civil Engineering Voice* 1, 122–138.

BS ISO 5168:2005 *Measurement of Fluid Flow – Procedures for the Evaluation of Uncertainties*. British Standards Institution. Available from: https://www.iso.org/obp/ui/#iso:std:iso:5168:ed-2:v1:en.

Downloaded from http://iwa.silverchair.com/jh/article-pdf/23/4/689/910515/jh0230689.pdf
by guest

BS ISO 1088:2007 *Hydrometry – Velocity-Area Methods Using Current-Meters – Collection and Processing of Data for Determination of Uncertainties in Flow Measurement*. British Standards Institution. Available from: https://www.iso.org/obp/ui/#iso:std:iso:1088:ed-3:v1:en.

CFD Simulation Software | ANSYS Fluids n.d. Available from: https://www.ansys.com/products/fluids (accessed 15 December 2020).

Draper, N. R. & Smith, H. 1998 *Applied Regression Analysis*, 3rd edn. John Wiley & Sons, Inc, New York.

Erdbrink, C. D., Krzhizhanovskaya, V. V. & Sloot, P. M. A. 2014 Free-surface flow simulations for discharge-based operation of hydraulic structure gates. *Journal of Hydroinformatics* **16** (1), 189–206. https://doi.org/10.2166/hydro.2013.215.

Garde, R. J., Ranga Raju, K. G. & Sujudi, A. W. R. 1990 Design of settling basins. *Journal of Hydraulic Research* **28** (1), 81–91. https://doi.org/10.1080/00221689009499148.

GR 500 Professional, Measuring Rod | Bosch n.d. Available from: http://www.bosch-professional.com/za/en/measuring-rod-gr-500-131504-0601094300.html (accessed 13 December 2020).

Herschy, R. W. 2009 *Streamflow Measurement*, 3rd edn. Routledge Taylor & Francis group. https://doi.org/10.4324/9780203931394.

Idel'chik, I. E. 1966 Stream flow through pipe fittings and labyrinth seals. In: D. Grunaer, ed. *Handbook of Hydraulic Resistance: Coefficients of Local Resistance and of Friction*. Isreal Program for Scientific Translations Ltd, Jerusalem. English version. AEC TR-6630, pp. 350–379.

ISO 748:2007 *Hydrometry – Measurement of Liquid Flow in Open Channels Using Current-Meters or Floats*. International Organization for Standardization (ISO). Available from: https://www.iso.org/standard/37573.html.

Issakhanian, E., Saez, J. A., Helmns, A. & Nickles, C. 2019 Full simulation of disinfection stage in a water recycling plant using low-cost, hybrid 3-dimensional computational fluid dynamics. *Water Environment Research* **91** (3), 177–184. https://doi.org/10.1002/wer.1020.

JDC Electronic SA – Flowatch n.d. Available from: https://www.jdc.ch/products/flow-meters/#flowatch (accessed 15 December 2020).

Karamarković, V., Nikolić, M., Karamarković, R. & Stojic, N. 2016 Optimization of the pipeline diameter for a small hydropower plant: case study. In: *XXXII International Conference Energetics*, pp. 265–274. Available from: https://www.researchgate.net/publication/323990553.

Karamarković, V. M., Nikolić, M. V., Karamarković, R. M., Karamarković, M. V. & Marašević, M. R. 2018 Techno-economic optimization for two SHPPs that form a combined system. *Renewable Energy* **122**, 265–274. https://doi.org/10.1016/j.renene.2018.01.081.

Khan, L. A., Wicklein, E. A. & Rashid, M. 2005 A 3D CFD model analysis of the hydraulics of an outfall structure at a power plant. *Journal of Hydroinformatics* **7** (4), 283–290. https://doi.org/10.2166/hydro.2005.0024.

May, R. W. P., Bromwich, B. C., Gasowski, Y. & Rickard, C. E. 2003 *Hydraulic Design of Side Weirs*. Thomas Telford. Available from: https://www.icevirtuallibrary.com/doi/book/10.1680/hdosw.31678.

Michelazzo, G., Oumeraci, H. & Paris, E. 2015 Laboratory study on 3D flow structures induced by zero-height side weir and implications for 1D modeling. *Journal of Hydraulic Engineering* **141** (10), 04015023. https://doi.org/10.1061/(asce)hy.1943-7900.0001027.

Neary, V. S. & Odgaard, A. J. 1993 Three-dimensional flow structure at open-channel diversions. *Journal of Hydraulic Engineering* **119** (9), 1223–1230. https://doi.org/10.1061/(ASCE)0733-9429(1993)119:11(1223).

Neary, V. S., Sotiropoulos, F. & Odgaard, A. J. 1999 Three-dimensional numerical model of lateral-intake inflows. *Journal of Hydraulic Engineering* **125** (2), 126–140. https://doi.org/10.1061/(ASCE)0733-9429(1999)125:2(126).

Nikolić, M. V., Karamarković, R. M., Karamarković, M. V. & Karamarković, V. M. 2021 Retrofit of a settling basin of a small hydropower plant. *Engineering Structures* **236**. https://doi.org/10.1016/j.engstruct.2021.112118.

Paschmann, C. 2018 *Design Optimization of Desanding Facilities for Hydropower Schemes*. Issue Diss. ETH No. 24913, ETH Zurich. https://doi.org/10.3929/ethz-b-000273062.

Paschmann, C., Fernandes, J. N., Vetsch, D. F. & Boes, R. M. 2017 Assessment of flow field and sediment flux at alpine desanding facilities. *International Journal of River Basin Management* **15** (3), 287–295. https://doi.org/10.1080/15715124.2017.1280814.

Ranga Raju, K. G., Kothyari, U. C., Srivastav, S. & Saxena, M. 1999 Sediment removal efficiency of settling basins. *Journal of Irrigation and Drainage Engineering* **125**, 308–314. https://doi.org/10.1061/(ASCE)0733-9437(1999)125:5(308).

Robinson, D. I. & McGhee, T. J. 1994 Computer modeling of side-flow weirs. *Journal of Irrigation and Drainage Engineering* **119** (6), 989–1005. https://doi.org/10.1061/(ASCE)0733-9437(1993)119:6(989).

Singh, K. K., Pal, M., Ojha, C. S. P. & Singh, V. P. 2008 Estimation of removal efficiency for settling basins using neural networks and support vector machines. *Journal of Hydrologic Engineering* **13** (3), 146–155. https://doi.org/10.1061/(asce)1084-0699(2008)13:3(146).

Solomatine, D. P. & Ostfeld, A. 2008 Data-driven modelling: some past experiences and new approaches. *Journal of Hydroinformatics* **10** (1), 3–22. https://doi.org/10.2166/hydro.2008.015.

Swamee, P. K. 1992 Sluice-gate discharge equations. *Journal of Irrigation and Drainage Engineering* **118** (1), 56–60. https://doi.org/10.1061/(asce)0733-9437(1992)118:1(56).

The Engineering ToolBox n.d. Available from: https://www.engineeringtoolbox.com/water-density-specific-weight-d_595.html (accessed 13 December 2020).

Vittal, N. & Raghav, M. S. 1997 Design of single-chamber settling basins. *Journal of Hydraulic Engineering* **123** (5), 469–471. https://doi.org/10.1061/(ASCE)0733-9429(1997)123:5(469).

First received 10 January 2021; accepted in revised form 5 April 2021. Available online 16 April 2021

Downloaded from http://iwa.silverchair.com/jh/article-pdf/23/4/689/910515/jh0230689.pdf
by guest